

Prediction for the Mass Spectra of Resonance Mesons in the Soft-Wall AdS/QCD with a Modified 5D Metric

Yan-Qin Sui, Yue-Liang Wu, Zhi-Feng Xie and Yi-Bo Yang

*Kavli Institute for Theoretical Physics China (KITPC)
Key Laboratory of Frontiers in Theoretical Physics
Institute of Theoretical Physics Chinese Academy of Sciences
Beijing, 100190, People's Republic of China*

Abstract

A soft-wall anti-de Sitter/QCD model with a modified five-dimensional metric at the infrared region is constructed to obtain a nontrivial dilaton solution, which incorporates the chiral symmetry breaking and linear confinement. By taking the pion mass and decay constant as two input mass scales, the resulting predictions for the resonance states of pseudoscalar, scalar, vector and axial-vector mesons agree remarkably with the experimentally confirmed resonance states. The effects of the quartic interaction term are investigated by taking an appropriate sign and magnitude for maintaining the stability of the bulk scalar potential. It is shown that such a simply modified soft-wall anti-de Sitter/QCD model can lead to a consistent prediction for the mass spectra of resonance states in the pseudoscalar, scalar, vector and axial-vector mesons; the agreement with the experimental data is found to be better than 10% for the excited meson states. The resulting pion form factor also agrees well with the experimental data.

PACS numbers: 12.40.-y,12.38.Aw,12.38.Lg,14.40.-n

I. INTRODUCTION

Strong interactions of quarks are described in the standard model by an $SU(3)$ gauge theory known as quantum chromodynamics (QCD) [1]. As the gauge group is non-Abelian, the gluons have direct self-interactions that lead to the well-known asymptotic freedom [2, 3] due to a negative beta function, $\beta(\mu)$, which causes the coupling constant $\alpha_s(\mu)$ to decrease at short distances (UV region), so that perturbative QCD at the UV region works well. At low energies (IR region), perturbative methods are no longer applicable as the coupling constant $\alpha_s(\mu)$ grows in the IR. We are currently unable to solve from first principle the low energy dynamics of QCD; one can then construct effective quantum field theories to describe the low energy features of QCD, such as dynamically generated spontaneous symmetry breaking [4]. It has been shown in Ref. [5] that such a dynamically generated spontaneous chiral symmetry breaking can lead to the consistent mass spectra for both the lowest lying nonet pseudoscalar mesons and nonet scalar mesons. Though the resulting mass spectra for the ground states were found to agree well with the experimental data, it is not manifest in a chiral effective field theory how to characterize the excited meson states.

It is well-known that there are two important features of QCD at the low energy: they are the chiral symmetry breaking and linear confinement. It was shown in [6] that for an $SU(N_c)$ QCD one may carry out a $1/N_c$ expansion in a large N_c limit. In this limit, theory remains maintaining the most important features such as color confinement and dynamical chiral symmetry breaking. Thus any consistent low energy QCD model should simultaneously characterize these two basic features. Besides that, the model should also practically be applicable to calculate the low energy quantities of QCD, such as the decay and coupling constants, the mass spectra of various meson resonances.

The duality between gravity and gauge theories conjectured by Maldacena [7] and further developed in [8, 9] has shed new light on solving the problem of strongly coupled gauge theories. Thus the anti-de Sitter/conformal field theory (AdS/CFT) conjecture is regarded as an important step in theoretical physics in the past ten years, which establishes the duality between the weak coupled supergravity in AdS_5 and the strong coupled $\mathcal{N} = 4$ super Yang-Mills, and thus makes the calculations in the strong coupled theory become feasible [10]. This feature has attracted a lot of attention recently. It is expected that an analogous duality holds between AdS and QCD, though the latter is not an exact conformal theory. There are two approaches to pursuing this duality: one is the so-called top-down approach [11] and the other is the bottom-up approach [12, 13]. The former starts with the string theory and varies the gravity background so as to reproduce the basic QCD features. The latter is inspired by the AdS/CFT conjecture and known as a phenomenological AdS/QCD model. The model consists of a gauge theory in a curved space (usually AdS) with the field contents chosen to holographically match some bound states and operators in QCD. It is also interesting to observe the correspondence between matrix elements obtained in AdS/CFT with the corresponding formula using the light-front representation as shown in

Refs. [14–16].

The current impressive achievements of AdS/QCD models contain the chiral symmetry breaking in a hard-wall AdS/QCD model [12] and the linear confinement in a soft-wall AdS/QCD model [17]. Nevertheless, in the hard-wall model [12], the resulting mass spectra for the excited mesons are contrary to the experimental data. In the soft-wall model [17], one can obtain a desired mass spectra for the excited vector mesons, while the chiral symmetry breaking phenomenon cannot consistently be realized. Note that a dilaton field in the soft-wall model is introduced by hand as a uniform background field. Interesting progress was made in Refs. [18, 19]: a quartic interaction term in the bulk scalar potential was introduced to incorporate linear trajectories and chiral symmetry breaking. Nevertheless, such a term was shown [19] to cause an instability of the scalar potential and result in a negative mass for the lowest lying scalar meson state and much smaller mass spectra for other lowest lying meson states in comparison with the experimental data. Thus how to naturally incorporate these two important features into a single AdS/QCD model and obtain the consistent mass spectra remains a challenging and interesting task.

On this note, we provide an alternative soft-wall AdS/QCD model by simply modifying the five-dimensional (5D) metric in the IR region. The paper is organized as follows: In Sec. II, we introduce the modified 5D soft-wall AdS/QCD model and show how the background dilaton field gets a desired IR behavior from a simply modified 5D metric; several phenomenological AdS/QCD models corresponding to different choices of the bulk vacuum expectation value (VEV) of the scalar field are considered. In Sec. III, we provide a detailed analysis and show how such simply modified soft-wall AdS/QCD models can simultaneously describe both chiral symmetry breaking and linear confinement, and lead to a reasonable prediction for the mass spectra of the various resonance states in the pseudoscalar, scalar, vector and axial-vector mesons. Unlike the predictions given in [19], the simply modified AdS/QCD model in our present considerations contains no virtual meson state in the scalar sector. In particular, the resulting resonance meson states agree well with the experimentally confirmed meson states and there are no more additional unconfirmed resonance meson states existing in the present model. The effects of a quartic interaction term in the bulk scalar potential are investigated in Sec. IV. By taking an appropriate sign (that is opposite to the one considered in [19]) for the coupling constant of the quartic interaction to keep the stability of the bulk scalar potential, we found that the resulting predictions for the mass spectra of resonance mesons can be further improved and consistent with the experimental data. Our conclusions and remarks are presented in the last section.

II. THE SOFT-WALL ADS/QCD MODEL WITH MODIFIED 5D METRIC

In the real world, QCD is known to be neither supersymmetry nor quantum mechanically conformal. Therefore, the 5D space of AdS in the AdS/QCD model is not necessary to be

a pure AdS. Here we shall consider the simplest extension to a 5D AdS with the following metric structure

$$ds^2 = a^2(z) (\eta_{\mu\nu} dx^\mu dx^\nu - dz^2); \quad a^2(z) = (1 + \mu_g^2 z^2)/z^2 \quad (1)$$

where $\eta_{\mu\nu} = \text{diag}(1, -1, -1, -1)$, and μ_g is a constant mass scale. Such a nonpure AdS space was also considered in [20] with a hard-wall cut. Here we shall show that in the soft-wall AdS/QCD with the above simply modified 5D metric at the IR region, it can lead to a consistent prediction for the mass spectra in the pseudoscalar, scalar, vector and axial-vector meson resonances. The effects of a quartic term in the bulk scalar potential are found to further improve the mass spectra of resonance mesons when taking an appropriate sign and magnitude for the coupling constant.

It has been shown in [17] that the introduction of a background dilaton Φ can lead to a linear trajectory for resonance vector meson mass once Φ has an asymptotic behavior

$$\Phi(z \rightarrow \infty) = \mu_d^2 z^2 \quad (2)$$

where the parameter μ_d sets the meson mass scale. The 5D action with the background field of dilaton $\Phi(z)$ and a quartic term in the bulk scalar potential can be written as follows

$$S_5 = \int d^5x \sqrt{g} e^{-\Phi(z)} \text{Tr} \left[|DX|^2 - m_X^2 |X|^2 - \lambda |X|^4 - \frac{1}{4g_5^2} (F_L^2 + F_R^2) \right] \quad (3)$$

with $g = |\det g_{MN}|$, $D^M X = \partial^M X - iA_L^M X + iX A_R^M$, $A_{L,R}^M = A_{L,R}^M{}^a t^a$ and $\text{Tr}[t^a t^b] = \delta^{ab}/2$. Here $A_{L,R}^M$ are introduced to gauge the chiral symmetry $SU(2)_L \times SU(2)_R$. λ is the coupling constant which has an opposite sign in comparison with the one in [19].

The parameter g_5 is fixed to be $g_5^2 = 12\pi^2/N_c$ [12] with N_c the color number and $m_X^2 = -3$ by AdS/CFT correspondence. The UV boundary condition for the gauge fields A_L and A_R at $z = 0$ is given by the value of the sources of the currents J_L and J_R in 4D theory as required by the holographic correspondence. The IR boundary condition with the background field dilaton playing the role of the smooth soft-wall cutoff simply requires that the action is finite at $z \rightarrow \infty$, so that the ambiguity of the choice of the IR boundary condition in a hard-wall theory [12] disappears in the soft-wall theory [17].

The VEV of X field in 5D space has the following form for the two flavor case

$$\langle X(z) \rangle = \frac{1}{2} v(z) \begin{pmatrix} 1 & 0 \\ 0 & 1 \end{pmatrix}.$$

For simplicity, we shall first consider the case with $\lambda = 0$. In this case, the VEV $v(z)$ satisfies the following condition

$$\partial_z (a^3(z) e^{-\Phi} \partial_z v(z)) - a^5(z) e^{-\Phi} m_X^2 v(z) = 0. \quad (4)$$

For the role played by X field on the boundary of AdS_5 [21], the VEV $v(z)$ has the following behavior at the UV boundary $z \rightarrow 0$:

$$v(z \rightarrow 0) = m_q \zeta z + \frac{\sigma z^3}{\zeta} \quad (5)$$

where m_q and σ are interpreted by AdS/CFT duality as the quark mass and quark condensate respectively. The normalization ζ is fixed by QCD with $\zeta = \sqrt{3}/(2\pi)$ [22]. The corresponding solution for the dilaton field at the UV boundary is found from Eq. (4) to be

$$\Phi'(z \rightarrow 0) = 6\mu_g^2 z + O(z^3), \quad \Phi(z \rightarrow 0) = 3\mu_g^2 z^2 + O(z^4) \quad (6)$$

The behavior of the VEV $v(z)$ in the IR boundary $z \rightarrow \infty$ is correlated to the dilaton behavior given in Eq. (2) which affects the mass spectra of meson resonances. In our present consideration with a modified metric given in Eq. (1), it is not difficult to find from Eq. (4) that a polynomial leading behavior for $v(z \rightarrow \infty)$ is enough to result in the required IR boundary condition for the dilaton background field. In general, we have the following IR boundary condition for $v(z)$

$$v(z \rightarrow \infty) = \gamma (\mu_d z)^\alpha, \quad (7)$$

with α being a positive parameter. Instituting the above boundary condition into Eq. (4), we can obtain a solution for the dilaton at the IR boundary:

$$\Phi'(z \rightarrow \infty) = \frac{3\mu_g^2}{\alpha} z, \quad \mu_d^2 = \frac{3}{2}\mu_g^2/\alpha \quad (8)$$

To investigate the dependence of the mass spectra of resonance mesons on the IR boundary conditions of the VEV $v(z)$, we are going to consider two interesting asymptotic behaviors of $v(z)$ at the IR boundary in three typical models which correspond to three different exact forms (I, II, III) of the VEV $v(z)$. One corresponds to $\alpha = 1$ as shown in the models Ia, IIa, IIIa, and the other to $\alpha = \frac{1}{2}$ as shown in the models Ib, IIb, IIIb. Explicitly, two different asymptotic behaviors of $v(z)$ are given by

$$\text{Case a : } v(z \rightarrow \infty) = \gamma (\mu_d z); \quad \text{Case b : } v(z \rightarrow \infty) = \gamma (\sqrt{\mu_d z}). \quad (9)$$

The explicit forms of $v(z)$ for three types of models (I, II, III) with two IR boundary conditions are summarized in the Table I. The three quantities m_q , σ and γ appearing in the boundary conditions of $v(z)$ are mainly correlated to the three parameters A , B and C (and G in IIIb case). The model III was shown to be a well parametrized one in the modified soft-wall model [19]. It will be shown below that the results in our present considerations are not very sensitive to the exact forms of the bulk VEV $v(z)$; they mainly depend on the IR boundary conditions. For a comparison, we plot in Fig. 1 the bulk VEV $v(z)$ for two

Models	$v(z)$	Parameters
Ia	$z(A + Bz^2)(1 + Cz^2)^{-1}$	$B = \frac{\sigma}{\zeta} + m_q\zeta C, C = B/\mu_d\gamma$
Ib	$z(A + Bz^2)(1 + Cz^2)^{-5/4}$	$B = \frac{\sigma}{\zeta} + \frac{5}{4}m_q\zeta C, C = (B^2/\mu_d\gamma^2)^{2/5}$
IIa	$z(A + Bz^2)(1 + Cz^4)^{-1/2}$	$B = \frac{\sigma}{\zeta}, C = (B/\mu_d\gamma)^2$
IIb	$z(A + Bz^2)(1 + Cz^4)^{-5/8}$	$B = \frac{\sigma}{\zeta}, C = (B^2/\mu_d\gamma^2)^{4/5}$
IIIa	$z[A + B \tanh(Cz^2)]$	$B = \mu_d\gamma - m_q\zeta, C = \frac{\sigma}{\zeta B}$
IIIb	$z[A + B \tanh(Cz^2)](1 + Gz^4)^{-1/8}$	$B = \mu_d^{1/2}\gamma G^{1/8} - m_q\zeta, C = \frac{\sigma}{\zeta B}$

TABLE I: Three type of models for $v(z)$ with two cases for each type of model and relevant parameters with $A = m_q\zeta$ for all the cases.

cases in model II. The corresponding dilaton field is plotted in Fig. 2 as the function of z . The three parameters m_q , σ and γ (or A , B and C) are fixed by the known experimental values of $m_\pi = 139.6$ MeV and $f_\pi = 92.4$ MeV with minimizing the breaking of the Gell-Mann-Oakes-Renner relation $f_\pi^2 m_\pi^2 = 2m_q\sigma$ at the 1% level. The parameter G is obtained by optimizing the mass spectra of vector and axial-vector mesons in model IIIb.

The pion decay constant is calculated from the axial-vector equation of motion with the pole in the propagator set to zero which was discussed in detail in Ref. [12]. Note that the axial-vector equation of motion depends on both quark mass and condensate. The pion decay constant is given [12]:

$$f_\pi^2 = -\frac{1}{g_5^2} \frac{\partial_z A(0, z)}{z} \Big|_{z \rightarrow 0}, \quad (10)$$

where $A(0, z)$ is the axial-vector bulk-to-boundary propagator and is obtained by solving the equation of motion in the momentum space

$$e^\Phi \partial_z (a(z) e^{-\Phi} \partial_z A(q, z)) + a(z) q^2 A(q, z) - a^3(z) g_5^2 v^2(z) A(q, z) = 0 \quad (11)$$

with $q^2 = 0$ and the boundary conditions $A(0, 0) = 1$ and $\partial_z A(0, z \rightarrow \infty) = 0$. The pion mass is related to the pseudoscalar equation of motion for the lowest lying state and will be discussed in Sec. III A.

III. MASS SPECTRA OF PSEUDOSCALAR, SCALAR, VECTOR AND AXIAL-VECTOR MESONS

In this section, we are going to make numerical calculations for the mass spectra of pseudoscalar, scalar, vector and axial-vector mesons. As μ_d or μ_g scales the mass spectra of meson resonances, it is not difficult to find out its value from a global fitting, the best value for the case $\lambda = 0$ is found to be

$$\mu_d = 445 \text{ MeV}; \quad \mu_g = 363 \text{ MeV} \quad (\text{Case a}), \quad \mu_g = 257 \text{ MeV} \quad (\text{Case b}) \quad (12)$$

The values of three fitting parameters m_q , σ and γ are presented in the Table II. The mass spectra for the pseudoscalar, scalar, vector and axial-vector resonance mesons are given in Tables III, IV, V and VI. All the quoted experimental data are taken from the particle data group (PDG) [23]. It is seen that the resonance states agree well with the experimentally confirmed states and the resulting mass spectra are consistent with the experimental values, except for the ground states of the scalar and axial-vector mesons which have masses smaller than the experimental data. The effects of a quartic interaction term in the bulk scalar potential are going to be studied in the next section and shown to be necessary for further improving the mass spectra.

Parameter	Ia	Ib	IIa	IIb	IIIa	IIIb
m_q (MeV)	4.16	4.64	4.44	4.07	4.98	4.25
$\sigma^{\frac{1}{3}}$ (MeV)	275	265	265	272	255	268
γ	0.178	0.136	0.153	0.112	0.164	0.112

TABLE II: The parameters m_q , σ and γ for $\lambda = 0$ in three type of models with two cases a and b corresponding to the IR boundary conditions given in Eq. (9).

A. Pseudoscalar Mesons

Writing the bulk scalar field as $X(x, z) \equiv (v(z)/2 + S(x, z))e^{2i\pi(x, z)}$ with $S(x, z)$ being the scalar meson field and $\pi(x, z) = \pi^a(x, z)t^a$ being the pseudoscalar meson field, and decomposing the axial field in terms of its transverse and longitudinal components, $A_\mu^a = A_{\mu\perp}^a + \partial_\mu\phi^a$, we then obtain, from the action Eq. (3), the following equation of motion in the 4D momentum space with the $A_5 = 0$ gauge:

$$\begin{aligned} \partial_z (a(z)e^{-\Phi}\partial_z\phi^a) + g_5^2 a^3(z)v^2(z)e^{-\Phi}(\pi^a - \phi^a) &= 0 \\ q^2\partial_z\phi^a - g_5^2 a^2(z)v^2(z)\partial_z\pi^a &= 0 \end{aligned} \quad (13)$$

By eliminating the longitudinal component field ϕ from the above coupled equation Eq. (13), we obtain the following equation for the π field

$$-\partial_z^2\tilde{\pi}(q, z) + V_\pi(z)\tilde{\pi}(q, z) = q^2\tilde{\pi}(q, z), \quad (14)$$

where $\tilde{\pi}(q, z) \equiv \partial_z\pi(q, z)$ and

$$\begin{aligned} V_\pi(z) &= g_5^2 a^2(z)v^2(z) + \frac{\Phi'^2 + 2\Phi''}{4} + \frac{15a'^2(z)}{4a^2(z)} - \frac{3a'(z)(v(z)\Phi' - 2v'(z))}{2a(z)v(z)} - \frac{3a''(z)}{2a(z)} \\ &+ \frac{2v'^2(z)}{v^2(z)} - \frac{\Phi'v'(z) + v''(z)}{v(z)}. \end{aligned} \quad (15)$$

Assuming $\tilde{\pi}(q, z) = \sum_n \Pi_n(q) \tilde{\pi}_n(z)$, we arrive at the following equation of motion

$$-\partial_z^2 \tilde{\pi}_n(z) + V_\pi(z) \tilde{\pi}_n(z) = m_{\pi_n}^2 \tilde{\pi}_n(z), \quad (16)$$

where q^2 is replaced by $m_{\pi_n}^2$ with m_{π_n} being the masses of pseudoscalar mesons. The above equation can be solved by the shooting method. Using the boundary conditions $\tilde{\pi}(z \rightarrow 0) = 0$, $\partial_z \tilde{\pi}(z \rightarrow \infty) = 0$, we obtain the mass spectra of excited states with the input of π mass and decay constant. The numerical results are given in Table. III and also plotted in Fig. 3. Where the mass of pion meson is as an input, the resulting excited meson states

n	π experimental. (MeV)	Ia	Ib	IIa	IIb	IIIa	IIIb
0	139.6	139.6	139.6	139.6	139.6	139.6	139.6
1	1350 ± 100	1219	1127	1285	1474	1339	1524
2	1816 ± 14	1632	1483	1664	1733	1721	1779
3	—	1949	1754	1960	1958	2015	1999
4	—	2218	1983	2212	2169	2264	2207
5	—	2455	2185	2444	2388	2491	2422
6	—	2670	2368	2677	2627	2717	2652
7	—	2869	2536	2923	2881	2956	2897

TABLE III: The experimental and predicted mass spectra for pseudoscalar mesons with $\lambda = 0$.

agree well with the data in models IIb, IIIa and IIIb. The agreement is seen to be within 10%; it is then interesting to provide a prediction for possible high excited states.

B. Scalar Mesons

Assuming $X(x, z) \equiv (v(z)/2 + S(x, z))e^{2i\pi(x, z)}$ and $S(x, z) = \sum_n \mathcal{S}_n(x)S_n(z)$, we arrive at the following equation of motion

$$\partial_z (a^3(z)e^{-\Phi} \partial_z S_n(z)) - a^5(z)e^{-\Phi} m_X^2 S_n(z) = -a^3(z)e^{-\Phi} m_{S_n}^2 S_n(z) \quad (17)$$

By defining $S_n(z) \equiv e^{\omega_s/2} s_n(z) = e^{(\Phi - 3 \log a(z))/2} s_n(z)$, we have

$$-\partial_z^2 s_n(z) + \left(\frac{1}{4} \omega_s'^2 - \frac{1}{2} \omega_s'' + a^2(z) m_X^2 \right) s_n(z) = m_{S_n}^2 s_n(z) \quad (18)$$

For simplicity, we consider here only the mass spectra for the $SU(3)$ singlet scalar mesons which have more experimental data.

Using the shooting method to solve Eq. (18) with the boundary conditions $s_n(z \rightarrow 0) = 0$, $\partial_z s_n(z \rightarrow \infty) = 0$, we obtain the mass spectra for the $SU(3)$ singlet resonance scalar mesons which are given in Table IV and also plotted in Fig. 3.

n	f_0 experimental. (MeV)	Ia	Ib	IIa	IIb	IIIa	IIIb
0	550_{-150}^{+250}	115	121	119	127	115	126
1	1350 ± 150	1002	1050	1099	1434	1122	1485
2	1724 ± 7	1366	1418	1446	1697	1468	1743
3	1992 ± 16	1644	1693	1713	1923	1734	1964
4	2189 ± 13	1877	1925	1939	2124	1958	2158
5	—	2083	2128	2140	2306	2155	2333
6	—	2268	2312	2321	2474	2333	2494
7	—	2440	2482	2489	2630	2497	2645

TABLE IV: The experimental and predicted mass spectra for the singlet scalar mesons with $\lambda = 0$.

It is seen that the resonance states agree well with the experimentally confirmed states though the ground state has a small mass (about 120 MeV) in comparison with the experimental data 550_{-150}^{+250} MeV, which have the biggest uncertainties. Note that this is unlike the model only considering a quartic interaction in the bulk scalar potential [19], where it was shown that the model may cause an instability and contains virtual mass for the lowest lying scalar meson. This is avoided in the present modified models which contain no virtual mass state. It must be clarified that the scalar states $f_0(980 \pm 10)$, $f_0(1505 \pm 6)$, $f_0(2103 \pm 8)$ and $f_0(2314 \pm 25)$ should be classified into the isosinglet resonance scalar states of $SU(3)$ octet mesons, rather than the $SU(3)$ singlet resonance scalar states. As an interesting check, we plot in Fig. 4 the corresponding bulk wave functions of $SU(3)$ singlet resonance scalar mesons; it is seen that the oscillation property becomes manifest in the scalar sector. Note that the possible instanton effects and the mixing effects between the $SU(3)$ singlet scalar and the isosinglet scalar of the $SU(3)$ octet are not included in the present considerations. It is manifest from Fig. 3 that the models IIb and IIIb lead to a better agreement with the experimental data.

C. Vector Mesons

From the action Eq. (3), with the gauge fixing $V_5 = 0$, one can derive the equation of motion for vector field

$$-\partial_z^2 V_n + \omega' \partial_z V_n = m_{V_n}^2 V_n, \quad (19)$$

For simplicity, we omit the Lorentz index and group index in flavor space. Defining $V_n \equiv e^{\omega/2} v_n = e^{(\Phi(z) - \log a(z))/2} v_n$, the above equation can be rewritten as

$$-\partial_z^2 v_n + \left(\frac{1}{4} \omega'^2 - \frac{1}{2} \omega'' \right) v_n = m_{V_n}^2 v_n. \quad (20)$$

Such an eigenvalue equation can also be solved by the shooting method, using the boundary conditions $v_n(z \rightarrow 0) = 0$, $\partial_z v_n(z \rightarrow \infty) = 0$; the resulting mass spectra are presented in Table.V and also plotted in Fig. 3. It is interesting to note that such a simple model can lead to a remarkable agreement with the experimental data, especially in the models IIb and IIIb. For an illustration, we also plot in Fig. 5 the bulk wave functions of the ground state and the excited state ($n = 4$) for various cases.

n	ρ experimental. (MeV)	Ia	Ib	IIa	IIb	IIIa	IIIb
0	775.5 ± 1	739	603	777	727	775	748
1	1465 ± 25	1223	1175	1292	1468	1303	1501
2	1720 ± 20	1534	1509	1596	1744	1610	1773
3	1909 ± 30	1784	1769	1842	1971	1856	1999
4	2149 ± 17	2000	1990	2054	2170	2068	2196
5	2265 ± 40	2193	2187	2249	2351	2255	2373
6	—	2370	2367	2417	2516	2426	2535
7	—	2534	2532	2578	2671	2584	2685

TABLE V: The experimental and predicted mass spectra for vector mesons with $\lambda = 0$.

D. Axial-vector Mesons

From the action Eq. (3) with the gauge $A_5 = 0$, one can derive the equation of motion for perpendicular component of axial field

$$e^{\Phi} \partial_z (a(z) e^{-\Phi} \partial_z A_n) + a(z) q^2 A_n - a^3(z) g_5^2 v^2(z) A_n = 0 \quad (21)$$

Again defining $A_n \equiv e^{\omega/2} a_n = e^{(\Phi(z) - \log a(z))/2} a_n$, the above equation of motion can be reexpressed as

$$-\partial_z^2 a_n + \left(\frac{1}{4} \omega'^2 - \frac{1}{2} \omega'' + g_5^2 v^2(z) a^2(z) \right) a_n = m_{A_n}^2 a_n. \quad (22)$$

With the boundary conditions $a_n(z \rightarrow 0) = 0$, $\partial_z a_n(z \rightarrow \infty) = 0$, the resulting mass spectra by using the shooting method is given in Table. VI and also plotted in Fig. 3. The resonance states agree well with the experimental ones, while the mass for the ground state is slightly smaller than the experimental data.

n	a_1 experimental. (MeV)	Ia	Ib	IIa	IIb	IIIa	IIIb
0	1230 ± 40	934	714	940	807	963	833
1	1647 ± 22	1468	1247	1496	1507	1539	1540
2	1930^{+30}_{-70}	1822	1573	1831	1778	1880	1807
3	2096 ± 122	2109	1829	2102	2003	2152	2031
4	2270^{+55}_{-40}	2358	2049	2338	2202	2386	2228
5	—	2582	2247	2549	2380	2594	2403
6	—	2787	2439	2742	2545	2785	2564
7	—	2979	2638	2922	2699	2964	2713

TABLE VI: The experimental and predicted mass spectra for axial-vectors with $\lambda = 0$.

IV. QUARTIC INTERACTION OF BULK SCALAR

It is interesting to note that the above simplest AdS/QCD model with four parameters can lead to a consistent prediction for all the experimentally confirmed resonance meson states, while the ground state masses of scalar and axial-vector mesons obtained above appear to be smaller than the experiment data though the lowest lying scalar mass has the biggest uncertainty. To make a possible improvement, we now turn to consider the effects of the quartic interaction $\lambda|X|^4$ in the bulk scalar potential. In this case, the equation for the VEV $v(z)$ is modified to be

$$\partial_z (a^3(z)e^{-\Phi}\partial_z v(z)) - a^5(z)e^{-\Phi}(m_X^2 + \frac{\lambda}{2}v^2(z))v(z) = 0. \quad (23)$$

and the equation of motion for the scalar field is extended to be

$$\partial_z (a^3(z)e^{-\Phi}\partial_z S_n(z)) - a^5(z)e^{-\Phi} \left(m_X^2 + \frac{3}{2}\lambda v^2(z) \right) S_n(z) = -a^3(z)e^{-\Phi} m_{S_n}^2 S_n(z) \quad (24)$$

Using the shooting method and making a global fitting with input mass scales of the π meson mass and decay constant as well as the Gell-Mann-Oakes-Renner relation, we present all the numerical results in Tables VIII, IX, X, XI and also plot them in Fig. 6. The model parameters are reanalyzed and given in Table VII. The reasonable value for the coupling constant λ is found to be $\lambda = 9$ and the parameter G in model IIIb is fitted to be $G = 0.01 \text{ GeV}^4$.

It is interesting to see that the inclusion of the quartic interaction term with an appropriate sign and magnitude can further improve the predictions. Especially, the models IIb and IIIb lead to a better agreement, which shows that the IR boundary condition $v(z \rightarrow \infty) \sim \sqrt{z}$ is more reasonable than the IR boundary condition $v(z \rightarrow \infty) \sim z$.

Parameter	IIa	IIb	IIIa	IIIb
m_q (MeV)	6.95	6.79	7.08	6.49
$\sigma^{\frac{1}{3}}$ (MeV)	228	229	226	233
γ	0.30	0.20	0.29	0.20
μ_d (MeV)	412	548	412	557

TABLE VII: The fitting parameters m_q , σ , γ , μ_d with $\lambda = 9$.

n	π experimental. (MeV)	IIa	IIb	IIIa	IIIb
0	139.6	139.6	139.6	139.6	139.6
1	1350 ± 100	1399	1526	1441	1437
2	1816 ± 14	1709	1871	1722	1824
3	—	1979	2103	1975	2080
4	—	2242	2295	2231	2283
5	—	2500	2493	2488	2482
6	—	2757	2716	2743	2704
7	—	3013	2960	2998	2948

TABLE VIII: The experimental and predicted mass spectra for pseudoscalar mesons with $\lambda = 9$.

n	f_0 experimental. (MeV)	IIa	IIb	IIIa	IIIb
0	550^{+250}_{-150}	493	317	495	305
1	1350 ± 150	1083	1401	1100	1307
2	1724 ± 7	1402	1757	1413	1708
3	1992 ± 16	1707	1986	1702	1964
4	2189 ± 13	1997	2158	1982	2154
5	—	2278	2290	2260	2297
6	—	2550	2373	2531	2392
7	—	2815	2434	2793	2448

TABLE IX: The experimental and predicted mass spectra for scalar mesons with $\lambda = 9$.

V. VECTOR COUPLING AND PION FORM FACTOR

As a useful check for the consistency of our present AdS/QCD model, we are going to perform a calculation for the vector coupling $g_{\rho\pi\pi}$ and the pion form factor $F_\pi(q^2)$. The

n	ρ experimental. (MeV)	IIa	IIb	IIIa	IIIb
0	775.5 ± 1	583	646	584	661
1	1465 ± 25	900	1468	893	1378
2	1720 ± 20	1248	1793	1252	1753
3	1909 ± 30	1564	2008	1565	1994
4	2149 ± 17	1860	2170	1847	2174
5	2265 ± 40	2143	2289	2122	2332
6	—	2417	2353	2395	2372
7	—	2685	2420	2661	2432

TABLE X: The experimental and predicted mass spectra for vector mesons with $\lambda = 9$.

n	a_1 experimental(MeV)	IIa	IIb	IIIa	IIIb
0	1230 ± 40	1128	913	1150	906
1	1647 ± 22	1643	1618	1668	1544
2	1930^{+30}_{-70}	1953	1940	1950	1903
3	2096 ± 122	2225	2161	2213	2146
4	2270^{+55}_{-40}	2486	2333	2473	2332
5	—	2742	2470	2726	2480
6	—	2993	2574	2974	2594
7	—	3239	2642	3217	2667

TABLE XI: The experimental and predicted mass spectra for axial-vector mesons with $\lambda = 9$.

vector coupling $g_{\rho\pi\pi}$ in the soft-wall AdS/QCD is given as follows[12]:

$$g_{\rho\pi\pi} = \frac{g_5}{N} \int dz V_\rho(z) e^{-\Phi(z)} \left(\frac{a(z)(\partial_z \varphi(z))^2}{g_5^2} + v^2(z)a^3(z)(\pi(z) - \varphi(z))^2 \right) \quad (25)$$

where $V_\rho(z)$ is the ρ meson bulk wave function corresponding to the vector meson bulk wave functions V_n with $n = 0$. Note that in all the integrals over z , the integration region is in principle the whole range $z \in (0, \infty)$. While in the practical calculations, for the lower limit, one can set a value as small as possible so as to obtain a stable result, for the upper limit, considering the suppressed factor $e^{-\Phi(z)}$, one can take at a certain finite value where the integrand tends to be zero. V_n satisfies the normalization condition:

$$\int dz a(z) e^{-\Phi(z)} V_n(z) V_m(z) = \delta_{mn}. \quad (26)$$

The functions $\pi(z)$ and $\varphi(z)$ are the solutions of Eq. (13) and normalized as follows:

$$N = \int dz e^{-\Phi(z)} \left(\frac{a(z)(\partial_z \varphi(z))^2}{g_5^2} + v^2(z)a^3(z)(\pi(z) - \varphi(z))^2 \right) \quad (27)$$

The numerical results are found to be $g_{\rho\pi\pi} = 3.63$ MeV (IIa), 2.94 MeV (IIb), 3.81 MeV (IIIa), 3.12 MeV (IIIb) with $\lambda = 0$. After including the quartic interaction with $\lambda = 9$, the results are changed to be $g_{\rho\pi\pi} = 2.86$ MeV (IIa), 3.51 MeV (IIb), 2.93 MeV (IIIa), 3.53 MeV (IIIb), which are still below the experimental value $g_{\rho\pi\pi} = 6.03 \pm 0.07$ MeV. Other soft-wall models also obtained small values, for instance, $g_{\rho\pi\pi} = 2.89$ in [19].

We now carry out a calculation for the spacelike pion form factor $F_\pi(q^2)$ by adopting the expressions in terms of the vector and axial-vector bulk-to-boundary propagators as given in [24]:

$$F_\pi(q^2) = \frac{g_5}{N} \int dz V(q, z) e^{-\Phi(z)} \left(\frac{a(z)(\partial_z \varphi(z))^2}{g_5^2} + v^2(z)a^3(z)(\pi(z) - \varphi(z))^2 \right) \quad (28)$$

where $V(q, z)$ is the vector bulk-to-boundary propagator which satisfies the following equation

$$-\partial_z^2 V(q, z) + \omega' \partial_z V(q, z) = q^2 V(q, z), \quad (29)$$

with the boundary condition $V(q, z \rightarrow 0) = 1$, so that $V(q, z)$ only depends on q^2 . The general considerations and derivations for the electromagnetic form factor in the AdS space can be seen in literature [25, 26], which may be compared with the corresponding light-front form given in [14–16]. Our result is plotted in Fig. 7 which shows a good agreement with the experimental data. It appears to be better than the one obtained in the AdS/QCD models considered in [19] and [24]. We would like to point out that though the coupling constant $g_{\rho\pi\pi}$ in Eq. (25) and the form factor F_π in Eq. (28) have a similar expression, the latter agrees well with the experimental data and the former has a discrepancy of about a factor of 2 with the experimental result. The reason is that the form factor is obtained by considering contributions from all resonance mesons rather than only from the ground state ρ meson, which may explicitly be seen from the following expression [24],

$$F_\pi(q^2) = - \sum_{n=1}^{\infty} \frac{f_n g_{n\pi\pi}}{q^2 - M_n^2}. \quad (30)$$

where the summation is over the ground state ρ meson and its excited states, f_n are related to their decay constants, $g_{n\pi\pi}$ are the corresponding coupling constants and M_n are their masses. It is noticed that the pion form factor is not sensitive to the IR boundary conditions, but it is relevant to the magnitude of quartic interaction. Thus more precise experimental measurement may be used to determine the coupling constant λ .

VI. CONCLUSION

In this paper, we have shown how the chiral symmetry breaking and linear confinement can be incorporated in the soft-wall AdS/QCD model by simply modifying the 5D metric

at the IR region. This is realized because a modification of the 5D metric at the IR region allows us to yield the desired IR and UV behaviors for the background dilaton field, so that the linear trajectories for the resonance meson states are simply obtained, and the resulting resonance meson states agree remarkably with the experimentally confirmed resonance states. It has also been shown that when a physically reasonable form of the bulk VEV is constructed to satisfy the boundary conditions of AdS_5 , the resulting mass spectra for all the resonance meson states are not very sensitive to the choice of the exact forms of the bulk VEV, which can be seen from the tables and figures of mass spectra by comparing among three models I, II and III. While the dependence of mass spectra on the IR boundary conditions of the bulk VEV has been shown to be significant for the scalar and vector mesons, and sizable for the pseudoscalar and axial-vector mesons, which can also be seen from the tables and figures of mass spectra by comparing two cases in each model, i.e., between Ia and Ib, IIa and IIb, IIIa and IIIb, the cases a and b correspond to the IR boundary conditions of bulk VEV $v(z \rightarrow \infty) \sim z$ and $v(z \rightarrow \infty) \sim \sqrt{z}$, respectively. It is concluded that the case b with the IR behavior $v(z \rightarrow \infty) \sim \sqrt{z}$ appears to provide more reasonable predictions for all the resonance mass spectra, which can be seen explicitly from Figs. 3 and 6.

The effects of the quartic interaction term have been investigated in detail; a physically reasonable sign of the coupling constant for the quartic interaction, which is opposite to the one considered in [19], is taken to avoid the possible instability of the bulk scalar potential. As a consequence, it has been found that the introduction of the quartic interaction with an appropriate sign and reasonable magnitude can result in a better agreement for the resonance mass spectra of scalar, pseudoscalar, vector and axial-vector mesons. Quantitatively, the agreement with the experimental data is found to be within 10% for all resonance meson states, though the predictions for the ground state mesons of scalar, vector and axial vector are not as good as the ones for the resonance states.

As such a simply modified soft-wall AdS/QCD model can result in such remarkable predictions for the mass spectra of resonance mesons, it would be interesting to further study the dynamical origin of the metric induced conformal symmetry breaking in the IR region. Also in the present consideration, the dilaton and gravity are treated as background fields; it would also be interesting to further investigate the important role of the dilaton field in connection with the stringy features of QCD and the 5D gravity effects from the back-reacted geometry which has been studied in a class of hard-wall AdS/QCD models [31]. It is a necessity to study the possible higher order interaction terms and their effects on the mass spectra and form factors of various mesons. It is also natural to extend to the three flavor case and consider the $SU(3)$ breaking and instanton effects.

Acknowledgements

This work was supported in part by the National Science Foundation of China (NSFC) under Grant #No. 10821504 and the Project of Knowledge Innovation Program (PKIP) of the Chinese Academy of Science.

- [1] H. Fritzsch, M. Gell-Mann and H. Leutwyler, *Phys. Lett. B* **47**, 365 (1973).
- [2] D. J. Gross and F. Wilczek, *Phys. Rev. Lett.* **30**, 1343 (1973).
- [3] H. D. Politzer, *Phys. Rev. Lett.* **30**, 1346 (1973).
- [4] Y. Nambu, *Phys. Rev. Lett.* **4** (1960) 380.
- [5] Y. B. Dai and Y. L. Wu, *Eur. Phys. J. C* **39** (2005) S1 [arXiv:hep-ph/0304075].
- [6] G. 't Hooft, *Nucl. Phys. B* **72**, 461 (1974).
- [7] J. M. Maldacena, *Adv. Theor. Math. Phys.* **2**, 231 (1998) [*Int. J. Theor. Phys.* **38**, 1113 (1999)] [arXiv:hep-th/9711200].
- [8] S. S. Gubser, I. R. Klebanov and A. M. Polyakov, *Phys. Lett. B* **428**, 105 (1998) [arXiv:hep-th/9802109].
- [9] E. Witten, *Adv. Theor. Math. Phys.* **2**, 253 (1998) [arXiv:hep-th/9802150].
- [10] J. Polchinski and M. J. Strassler, *Phys. Rev. Lett.* **88** (2002) 031601 [arXiv:hep-th/0109174].
- [11] T. Sakai and S. Sugimoto, *Prog. Theor. Phys.* **113**, 843 (2005) [arXiv:hep-th/0412141].
- [12] J. Erlich, E. Katz, D. T. Son and M. A. Stephanov, *Phys. Rev. Lett.* **95**, 261602 (2005) [arXiv:hep-ph/0501128].
- [13] L. Da Rold and A. Pomarol, *Nucl. Phys. B* **721** (2005) 79 [arXiv:hep-ph/0501218].
- [14] S. J. Brodsky and G. F. de Teramond, *Phys. Rev. Lett.* **96** (2006) 201601 [arXiv:hep-ph/0602252].
- [15] S. J. Brodsky and G. F. de Teramond, *Phys. Rev. D* **77**, 056007 (2008) [arXiv:0707.3859 [hep-ph]].
- [16] S. J. Brodsky and G. F. de Teramond, arXiv:0909.3899 [hep-ph]; G. F. de Teramond and S. J. Brodsky, arXiv:0909.3900 [hep-ph] and references therein.
- [17] A. Karch, E. Katz, D. T. Son and M. A. Stephanov, *Phys. Rev. D* **74**, 015005 (2006) [arXiv:hep-ph/0602229].
- [18] P. Colangelo, F. De Fazio, F. Giannuzzi, F. Jugeau and S. Nicotri, *Phys. Rev. D* **78** (2008) 055009 [arXiv:0807.1054 [hep-ph]].
- [19] T. Gherghetta, J. I. Kapusta and T. M. Kelley, *Phys. Rev. D* **79** (2009) 076003 [arXiv:0902.1998 [hep-ph]].
- [20] J. P. Shock and F. Wu, *JHEP* **0608** (2006) 023 [arXiv:hep-ph/0603142].
- [21] I. R. Klebanov and E. Witten, *Nucl. Phys. B* **556**, 89 (1999) [arXiv:hep-th/9905104].
- [22] P. H. Damgaard and H. Fukaya, *JHEP* **0901**, 052 (2009) [arXiv:0812.2797 [hep-lat]].

- [23] C. Amsler *et al.* [Particle Data Group], Phys. Lett. B **667** (2008) 1.
- [24] H. J. Kwee and R. F. Lebed, Phys. Rev. D **77**, 115007 (2008) [arXiv:0712.1811 [hep-ph]].
- [25] J. Polchinski and M. J. Strassler, JHEP **0305**, 012 (2003) [arXiv:hep-th/0209211].
- [26] H. R. Grigoryan and A. V. Radyushkin, Phys. Rev. D **76**, 115007 (2007) [arXiv:0709.0500 [hep-ph]].
- [27] V. Tadevosyan *et al.* [Jefferson Lab F(pi) Collaboration], Phys. Rev. C **75**, 055205 (2007) [arXiv:nucl-ex/0607007].
- [28] T. Horn *et al.* [Jefferson Lab F(pi)-2 Collaboration], Phys. Rev. Lett. **97**, 192001 (2006) [arXiv:nucl-ex/0607005].
- [29] H. Ackermann *et al.*, Nucl. Phys. B **137**, 294 (1978).
- [30] P. Brauel *et al.*, Phys. Lett. B **69**, 253 (1977).
- [31] J. P. Shock, F. Wu, Y. L. Wu and Z. F. Xie, JHEP **0703** (2007) 064 [arXiv:hep-ph/0611227].
Y. L. Wu and Z. F. Xie, JHEP **0710** (2007) 009 [arXiv:0705.2360 [hep-ph]].

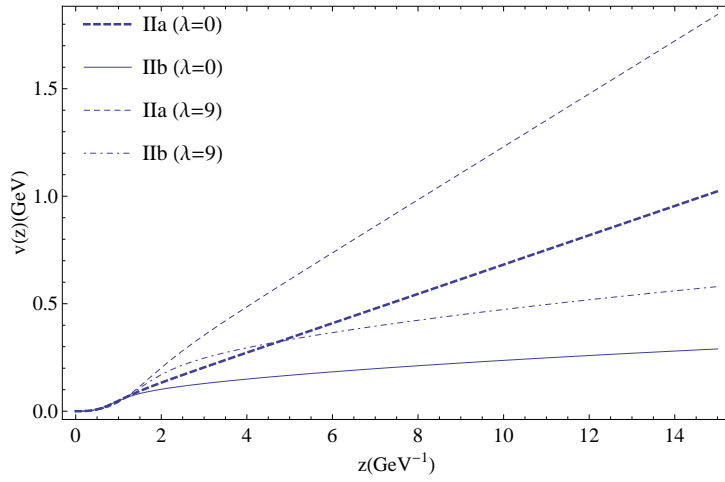


FIG. 1: A plot of $v(z)$ for various parameters which is fitted to the mass spectra.

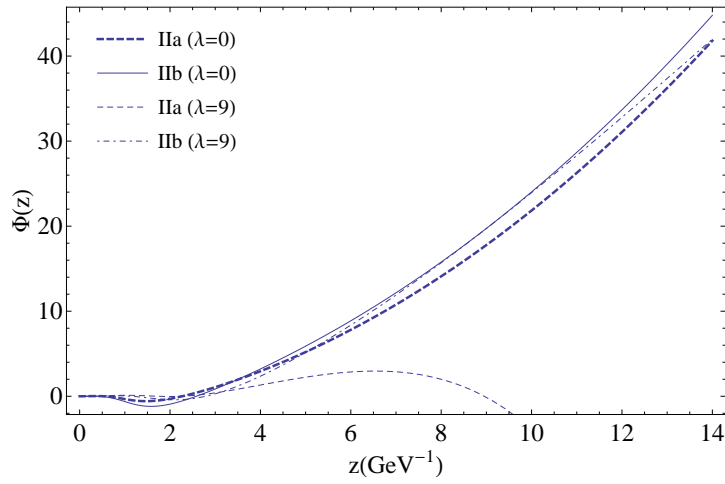


FIG. 2: A plot of dilation $\Phi(z)$ for various parameters fitted to the mass spectra

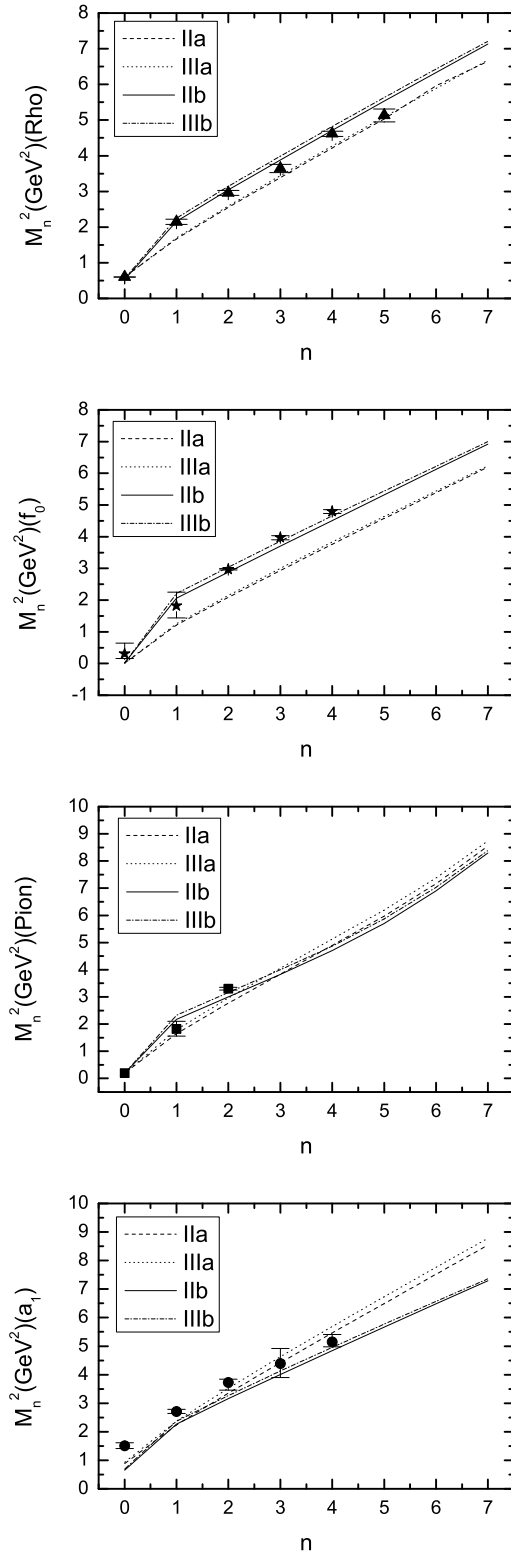


FIG. 3: A plot of mass spectra of resonance mesons in models IIa($\lambda = 0$), IIIa($\lambda = 0$), IIb($\lambda = 0$), IIIb($\lambda = 0$). The squares are the experimental mass spectra for the resonance pseudoscalars (π), the triangles for the resonance vector mesons (ρ), the circles for the resonance axial-vector mesons (a_1), and the stars are for the resonance scalar mesons (f_0).

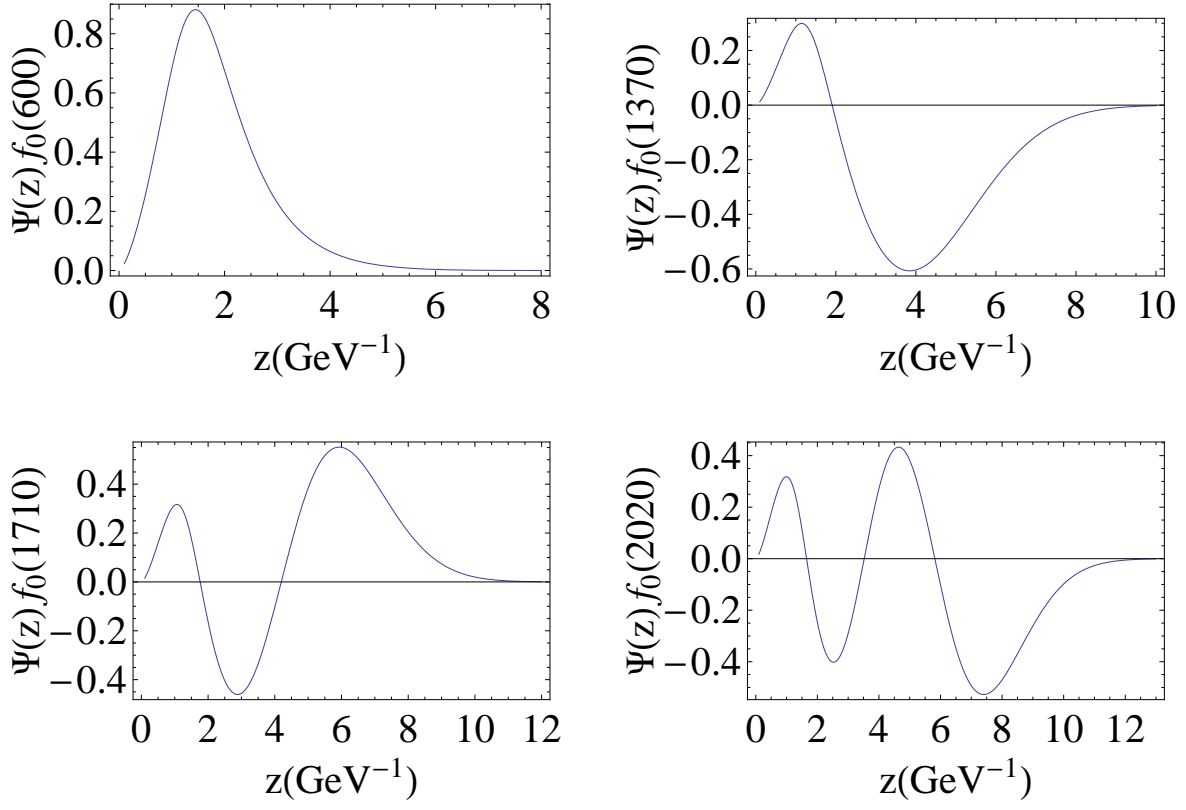


FIG. 4: Normalized bulk wave function for scalar mesons in case IIb($\lambda = 0$).

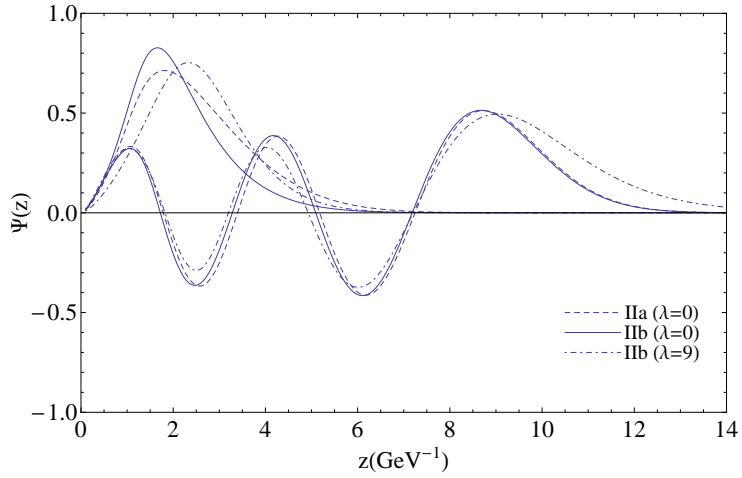


FIG. 5: Normalized bulk wave function for vector mesons with the single peak curve for the bulk wave function of ground state ρ and multipicks for the excited vector meson corresponding to $n = 4$.

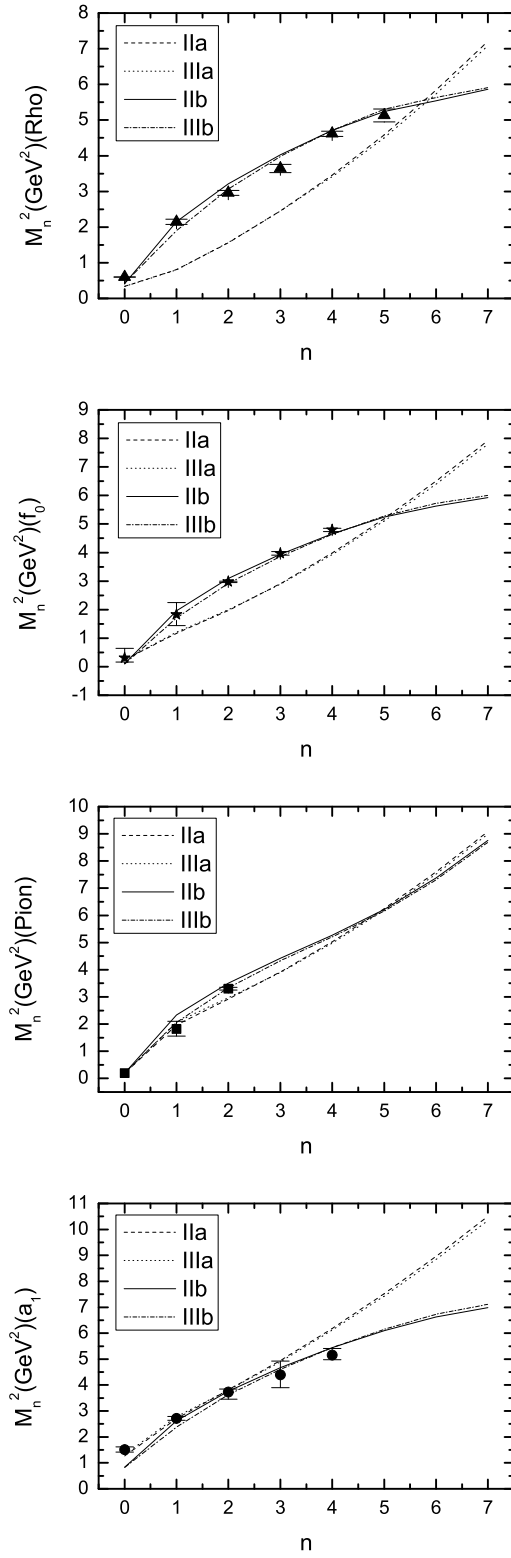


FIG. 6: Similar to Fig. 3, a plot of mass spectra of resonance mesons in models IIa($\lambda = 9$), IIIa($\lambda = 9$), IIb($\lambda = 9$), IIIb($\lambda = 9$).

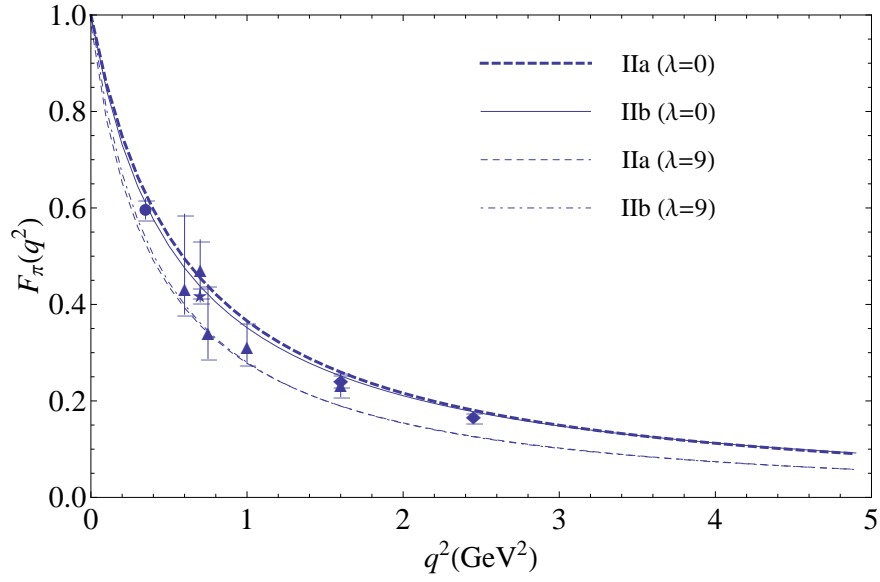


FIG. 7: The predicted spacelike behavior of the pion form factor $F_\pi(q^2)$ compared to the experimental data analyzed in [24]. The triangles are data from DESY, reanalyzed by [27]. The diamonds are data from Jefferson Lab [28]. The circle [29] as well as the star [30] are also data obtained from DESY.